PHILIPPINE ENGINEERING JOURNAL
PEJ 2007; **Vol. 28 No. 1**:57–76

Modeling of Cross-shore Wave Propagation with Moving Shoreline

Eric C. Cruz[1,*]

[1] *Institute of Civil Engineering, University of the Philippines, Diliman, Quezon City 1101, Philippines*

ABSTRACT

A numerical model for the transformation of nonlinear waves in the cross-shore direction towards the shore is developed by incorporating a moving shoreline boundary condition. The shoreline formulation is based on the net volumetric change effected by the translating shoreline front. Initial numerical results indicated the need to recast the (η, u) wave model to a (η, Q) form to remove the numerical instabilities due to discretization of the physical shoreline condition. It is also imperative to apply a threshold depth at the moving front to avoid singularities due to the very small total depth at the last wet point. Subsequent numerical simulations of nonbreaking wave runup on a plane sloping beach indicate that the moving boundary treatment reproduces the important wave evolution features revealed by past analytic studies. Results of numerical simulations of wave runup-rundown induced by nonlinear incident waves on beach slopes as high as 1/20 show the applicability of the moving shoreline treatment and the reformulated wave model.

1. INTRODUCTION

Wave models are indispensable tools in understanding many processes occurring in the nearshore zone of a coastal area. For example, wave models are now widely used to study and quantify the wave data needed by coastal engineers to assess the wave climate in beaches, bays, and similar sea-exposed bodies of water. They are also used to obtain information necessary to perform an engineering design of coastal structures such as breakwaters. Although many of these required data may be computed using applicable closed-form formulas, it is generally difficult to do so for more complex conditions of the sea bottom topography, shoreline plan-form and incident wave conditions, among others. Wave models are differential equations expressing the underlying physics of the wave evolution processes and are thus likely to reproduce these processes when appropriately codified.

Wave processes in the coastal area can generally be grouped into cross-shore or longshore, and the rest are combinations of these two. The shore is a dynamic feature of a coast that responds more quickly to cross-shore than to longshore processes. Examples of these processes are the shoaling of waves, wave breaking, wave set-up and wave-induced currents. Many of the longshore processes depend on the cross-shore processes, such as the inducement of longshore

*Correspondence to: Institute of Civil Engineering, University of the Philippines, Diliman, Quezon City 1105, Philippines. Email: eric.cruz@up.edu.ph

Received July 20, 2008
Revised September 14, 2009
Accepted December 18, 2009

currents and the generation of edge waves. Indeed, cross-shore processes need to be understood first in studying wave-related physical processes in the nearshore zone.

The movement of the shoreline in the swash zone is an important physical process that is responsible for many phenomena in the nearshore area. Among these are the modulation of the wave amplitude, the migration of the wave breaking point and the generation of low-frequency waves in shallow water. In order to accurately predict the physical processes in the nearshore zone, it is important to impose a moving shoreline condition in wave models. As this moving boundary will simulate the alternating immersed and dry conditions of the beach, its numerical implementation must be accurate and stable. Accuracy is required because of the small depths at the shore on which the wave evolution process primarily depends. Stability is also necessary to allow a long-duration simulation of real irregular waves involving numerous frequency components. Finally, the numerical implementation must also be computationally efficient so that memory and computation time are not very prohibitive.

1.1. Objectives

The main objective of this research is to develop a numerical model of the wave field in the cross-shore direction that considers the moving shoreline. An immediate objective is a model for the cross-shore direction without breaking waves. The present model purposely neglected the energy-dissipative wave transformations in shallow water such as wave breaking and oscillatory bottom friction in order to compare the model results with known analytical solutions based on such idealization. These physical processes can be incorporated into the present wave propagation model in a modular manner which will allow the model's validation based on empirical data; these will be the focus of the subsequent module of this research.

1.2. Review of Literature

There are two methods of incorporating a moving shoreline in wave field simulations. The first is by using a fixed spatial grid, and the second is through the so-called "moving grid" model. The first method has the main advantage that the governing equations can be coded with ease and efficiency. Its main disadvantage is that the moving water surface will cause grid points in the swash zone to change from being inundated to being dry in alternating fashion. In the second method, the grid points move with the shore boundary so that the shore-most point is always inundated. It main disadvantage lies in the difficulty of using variable grid spacing required by the variable location of the shoreline.

Studies employing the fixed grid approach are available in the literature. Reid and Bodine [4] proposed a procedure in which dry land becomes wet when the water surface elevation exceeds the still-water level. To determine whether the next shoreward point will become wet or remain dry in the next time level, Hibbert and Peregrine [2] applied extrapolation in the most shoreward wet grid point. In succeeding time steps, this grid point may become dry when the total water depth above it becomes lower than a certain threshold value. This procedure is repeated for the next wet point at succeeding time steps. Adopting a similar approach, Kobayashi and Johnson [3] later improved on it by addressing the tendency of the boundary condition to become unstable. However, their resulting procedure became quite complicated to be useful. Brocchini and Peregrine [1] presented a theoretical outline for the shoreline boundary, but did not include an application of the theory. A different technique was applied in Kennedy et al. [7], where a "slotted" beach is used to simulate the alternate wetting and drying of the

slope. However, the parameters of the slot are not easily determined and the concept may not be readily extendible to the horizontal 2D case.

In this study, a procedure based on the principle of placing a given volume of water between the last immersed point and the shoreline boundary is used to determine where the dry land for the next time level will commence. The procedure will be first applied to cross-shore propagation and will be compared with the nonlinear analytical solution by Carrier and Greenspan [11].

2. THE CROSS-SHORE WAVE MODEL

A special case of the horizontally two-dimensional Boussinesq-type equations of Cruz et al. [5] is used as the wave model in this study. Only the cross-shore direction is of interest and the seabed is treated as a solid boundary, *i.e.* impermeable to fluid particles, so that the following special case of the general horizontal 2D model for impermeable bottoms can be used for the one-dimensional (cross-shore) wave transformation:

$$\eta_t + [(h+\eta)u]_x = 0 \tag{1}$$

$$\begin{aligned} &u_t + \frac{1}{2}\left(u^2\right)_x + g\eta_x + \frac{1}{6}h^2 u_{txx} - \left(\frac{1}{2}+\gamma\right)h(hu_t)_{xx} \\ &-\gamma g h(h\eta_{xx})_x - \gamma g h h(h_x\eta_x)_x + \frac{f_w|u|}{2(h+\eta)^2}u + \epsilon u = 0 \end{aligned} \tag{2}$$

where u is the depth-averaged fluid particle horizontal velocity along the cross-shore direction x, t time, η the water surface elevation from still-water level, h the local water depth reckoned from still water, γ the dispersivity factor, g the gravity acceleration, f_w the friction factor for waves, and ϵ the boundary damping coefficient used in the open-boundary treatment. Subscripts t and x denote partial differentiation with respect to time and space, respectively.

By using $\gamma = 1/15$, it has been shown that the frequency dispersion range of the model equations extends from shallow waters to the deepwater limit (Cruz et al. [5]). Eqs. (1)-(2) can be solved for the unknown η and velocity u at the grid points for a given bathymetry $h(x)$, prescribed incident wave field (η_{in}, u_{in}), subject to the physical conditions at the lateral boundaries.

3. NUMERICAL IMPLEMENTATION OF THE WAVE MODEL

The physical process of interest in this study is the evolution of surface waves as they approach the swash zone where they run up and down the slope. Figure 1 shows the cross-shore transformation process in the physical domain along the direction of wave propagation, commencing from the offshore region on the left, to the shore on the right. Incident waves are introduced by a wave generator at the source $x = x_s$, which then propagate to the right and induce the migration of the shoreline at the beach. The technique of introducing a wave source at $x = x_s$ is similar to that of Ishii et al. [6]. However, in view of the nonlinear wave model used here, the resolution of the left-bound outgoing wave component simultaneously introduced at

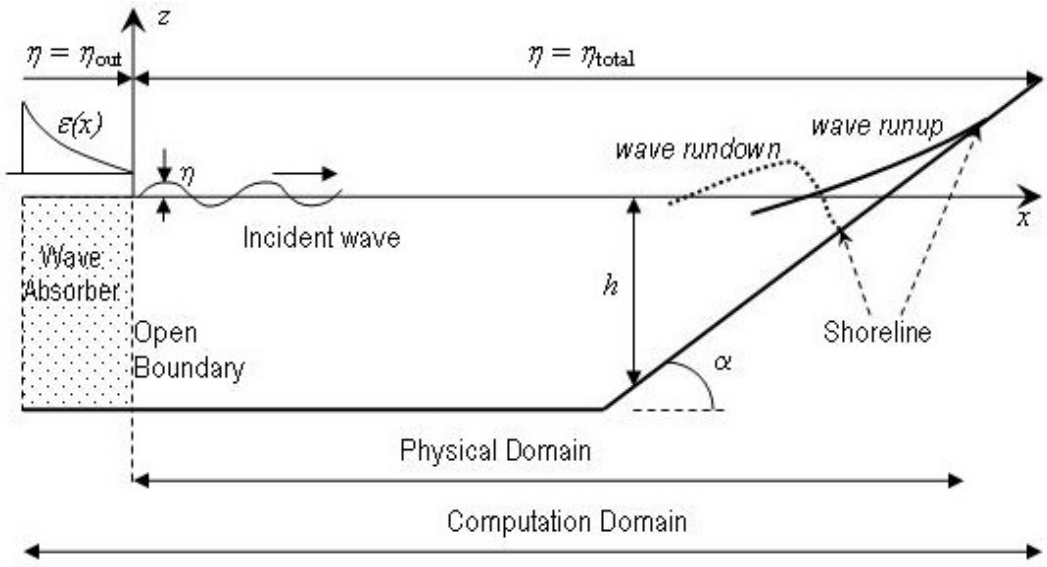

Figure 1. Definition sketch

the source is applied to both the η and u fields. This enhanced wave source technique allows the generation of weakly nonlinear incident waves without the undesirable bound harmonics that usually accompany linear wave models.

The physical domain usually generates reflected waves through, for example, natural reflection from structures in the interior. In the present study, the reflected wave may be generated by the swash motion in the foreshore slope itself and by the partial reflection induced by the runup slope. In any case, these outwardly propagating reflected waves must be allowed to move out of the physical domain. The seaward boundary of the domain is a physical open boundary where outgoing waves are allowed to completely pass through. This boundary condition is treated via the numerical wave absorption technique in conjunction with the Sommerfeld radiation condition (Cruz [8]). For purposes of numerical implementation of the wave model and treatment of the open-boundary condition at the seaward boundary, the variable η in the physical domain refers to the total η, *i.e.* composite incident and reflected waves. In the offshore absorption region of Figure 1, η refers to the outgoing wave only, *i.e.* $\eta_{out} = \eta - \eta_{in}$. The parameters of the numerical wave absorber are taken from the simulation aid graphs developed in Cruz [8]. These are the boundary damping distribution $\epsilon(x)$, damping length, and damping coefficient.

The computational grid is shown in Figure 2. For the cross-shore wave propagation considered here, the horizontal grid represents the propagation direction and the vertical the time axis. On the main grid (solid grid lines), the discrete values of $\eta(x,t)$ are solved. A secondary grid staggered relative to the main grid is used to compute the $u(x,t)$ values. The still-water depths $h(x)$ and total depths $D(x,t) = h(x) + \eta(x,t)$ are defined on the main grid. The use of a staggered grid has been found to be effective in eliminating the artificial viscosity associated with the use of non-staggered grids in highly inertial hydrodynamic models (Isobe

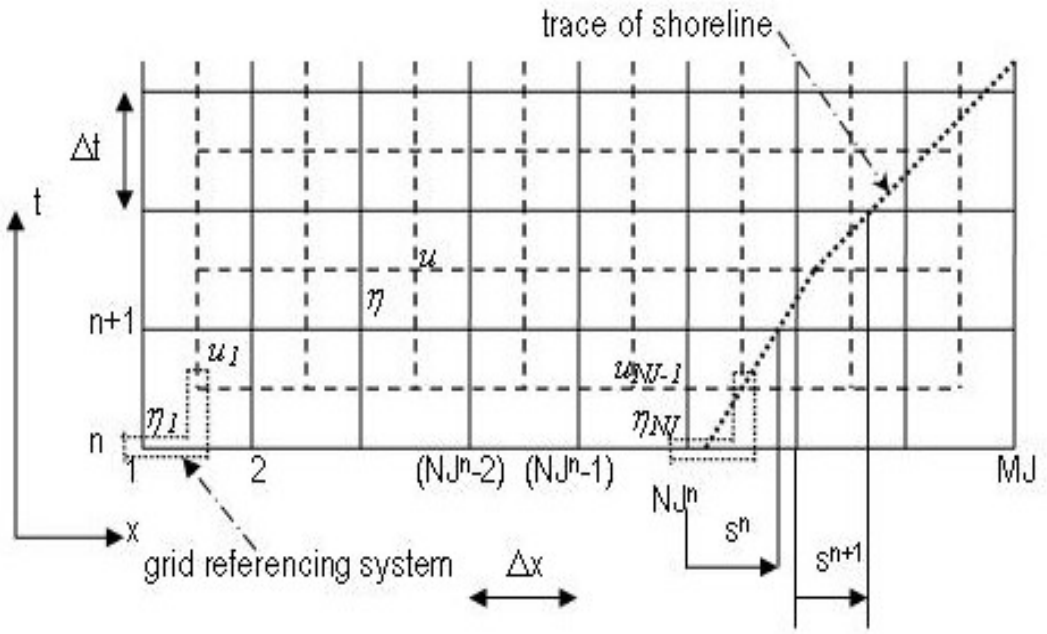

Figure 2. Computational grid

et al. [13], Madsen and Sorensen [12]). The maximum number of spatial grid is MJ, and the location of the last wet point (LWP) at any time is indexed by $j = NJ^n$. The grid spacing is Δx and the time step is Δt. The grid referencing system is also shown in Figure 2 where the last u-grid is $(NJ - 1)$ and the last η-grid is NJ. The time grid of u is at $(n + 1/2)\Delta t$.

Eqs. (1) and (2) are solved using a 3-point finite-difference stencil with an implicit scheme. This leads to a tridiagonal structure of the resulting system matrices which can be efficiently solved using high-accuracy, direct, in-place, reduction solution algorithms.

4. FORMULATION OF MOVING SHORELINE

The motion of the shoreline can be captured via a pseudo-control volume formulation by considering the change of oscillatory volumetric flow rate between time instances t^n and t^{n+1}. Figure 3 is a definition sketch of the variables used in the treatment of the moving shoreline. The shoreline position at any time is reckoned from the last wet point $x = x_o$ and may move up or down in the next instance. The actual shoreline position at time t^n is s^n. The problem essentially involves tracking the new position s^{n+1} in the next time level. The following describes the formulation for the moving shoreline condition.

First, the oscillatory flow volume V between consecutive time levels is defined as

$$V = \int_{t^n}^{t^{n+1}} Q|_{x_o} dt \tag{3}$$

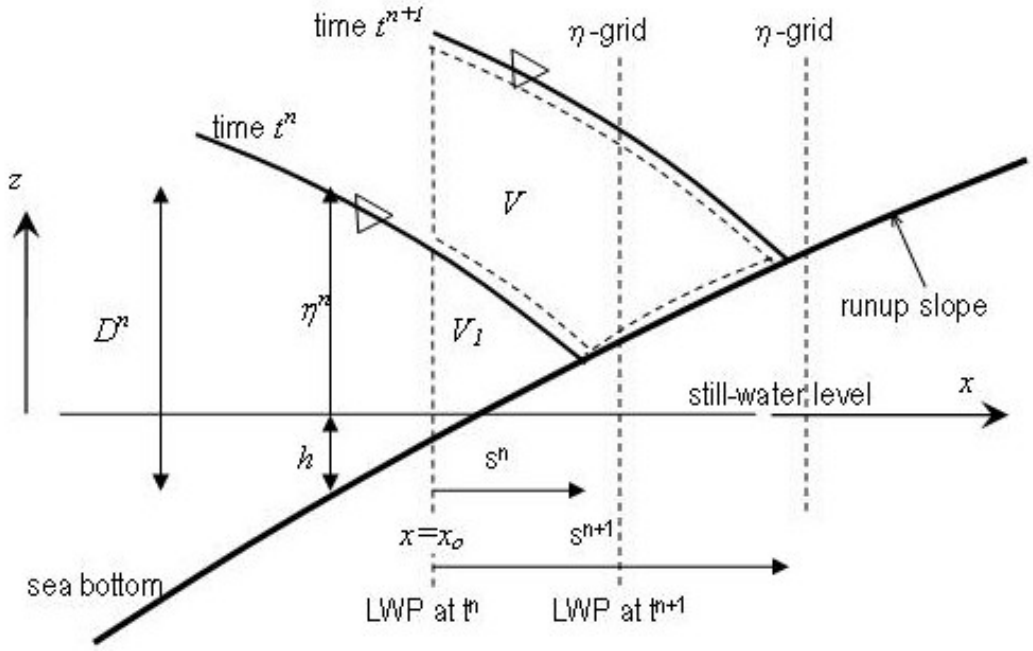

Figure 3. Definition sketch for moving shoreline

where Q is the wave-induced oscillatory flow rate (per unit width along y). The stored volume of water V_1 between time instances t^n and t^{n+1} can be derived based on the instantaneous slopes of the water surface and sea bottom, leading to:

$$V_1 = -\frac{(h+\eta^n)^2}{2\left(\dfrac{\partial h}{\partial x}+\dfrac{\partial \eta^n}{\partial x}\right)}. \tag{4}$$

The shoreline distance from the last wet point $x = x_o$ can be obtained from a direct solution for the intersection of the two surfaces:

$$s^n = -\frac{h+\eta^n}{\dfrac{\partial h}{\partial x}+\dfrac{\partial \eta^n}{\partial x}}. \tag{5}$$

The new displacement of the last wet point at the next time step is obtained by considering the net volume change between these times, yielding

$$\eta^{n+1} = \sqrt{-2(V+V_1)\left(\frac{\partial h}{\partial x}+\frac{\partial \eta^n}{\partial x}\right)} - h. \tag{6}$$

It is assumed in the preceding three equations that the water surface remains parallel to each other during this interval, *i.e.*

$$\frac{\partial \eta^{n+1}}{\partial x} \cong \frac{\partial \eta^n}{\partial x}. \tag{7}$$

This assumption results in the decoupling of the solutions for s^{n+1} and η^{n+1}, which simplifies the numerical solution of the updated shoreline.

The new shoreline position can be determined by relating the net flow volume $(V + V_1)$ to the kinematic conditions of the free surface at the LWP, yielding

$$s^{n+1} = \sqrt{-\frac{2(V_1 + V)}{\dfrac{\partial h}{\partial x} + \dfrac{\partial \eta^n}{\partial x}}} \tag{8}$$

The condition of wave runup or rundown is determined based on the sign of volume change $(V_1 + V)$, namely, runup occurs when $(V_1 + V) > 0$ and rundown otherwise.

In terms of the fluid particle velocity, the physical condition at the shoreline is expressed as

$$u_{sh} = 0 \text{ at } x = x_{sh} = x^n_{NJ} + s^n \tag{9}$$

5. NUMERICAL TREATMENT OF MOVING SHORELINE

The formulation above is integrated into the model equations (1) and (2) as a boundary condition. First, the flow rate is defined in terms of the main variables as follows:

$$\begin{aligned} Q_0 &= Q|_{x_0} = \tilde{u}(h + \eta) \\ &= \tilde{u}D \end{aligned} \tag{10}$$

where $\tilde{u}$ is the time-averaged velocity between t^n and t^{n+1} at $x = x_0$, Q_0 and D are the flow rate and total depth, respectively, at the last wet point. Then the incremental volume between times t^n and t^{n+1} can be evaluated on-grid as

$$\begin{aligned} V &= \int_{t^n}^{t^{n+1}} \tilde{u}(h + \eta)dt \\ &= \frac{3u^{n+1/2}_{NJ-1} - u^{n+1/2}_{NJ-2}}{2} \left[h_{NJ} + \frac{1}{2}\left(\eta^n_{NJ} + \eta^{n+1}_{NJ}\right)\right] \Delta t \end{aligned} \tag{11}$$

By linearly interpolating u_{NJ-1} between u_{NJ-2} and u_{sh}, the following algebraic equation is used for the last row entry of the u system matrix:

$$a_{-2}u^{n+1/2}_{NJ-2} + a_{-1}u^{n+1/2}_{NJ-1} = -a_{-2}u^{n-1/2}_{NJ-2} - a_{-1}u^{n-1/2}_{NJ-1} \tag{12}$$

where the unknowns are $u^{n+1/2}_{NJ-2}, u^{n+1/2}_{NJ-1}$. The right side is known for a previous time level $n, n - 1/2$, and the coefficients are

$$\begin{aligned} a_{-2} &= -\frac{2s^n + \Delta x}{2s^n + 3\Delta x}\left[h_{NJ-3/2} + \frac{1}{2}(\eta^n_{NJ-2} + \eta^n_{NJ-1})\right] \\ a_{-1} &= h_{NJ-1/2} + \frac{1}{2}(\eta^n_{NJ-1} + \eta^n_{NJ}) \end{aligned} \tag{13}$$

Starting from known conditions of η^n and $u^{n-1/2}$, the new shoreline position is determined sequentially as follows:

1. η_{NJ}^{n+1} is determined using Eq. (6).
2. The incremental volume V is evaluated using Eq. (11).
3. The updated shoreline position s^{n+1} is solved using Eq. (8).

This shoreline model has been integrated into the wave module, then tested on a runup bathymetry consisting of a horizontal bottom with a plane sloping beach. Figure 4 shows the results for the instantaneous spatial profiles of η and u. Note that the variables are normalized by the following properties of the incident wave: H_{in} wave height, L_{in} wavelength, T_{in} wave period and $u_{in} = (CH)_{in}$ the amplitude of particle horizontal velocity, in which C_{in} is wave celerity. Note that bottom friction is initially neglected in the simulations

Figure 4 indicates that the spatial profiles of η are correctly predicted by the model for the case of a plane sloping beach, where the wave runup in the swash zone induces a long wave component that interacts with the main wave. This interaction manifests as partial standing waves with increasing amplitudes toward the shore. The envelopes are also consistent with the theoretical profiles of Carrier and Greenspan [11]. However, some parasitic waves are unfortunately introduced into the numerical model, resulting in the confused waveforms of Figure 4. These undesirable waves will eventually lead to numerical instability, so that a long-duration simulation is not possible with the present model.

Figure 5 shows the local conditions close to the runup slope for the profiles shown in Figure 4, including the spatial envelopes of η after about 15 wave periods. The spatial profiles of η every $T_{in}/8$ intervals clearly indicate that the parasitic waves become prominent at times when the shoreline is very close to its still-water position.

To solve the problem of numerical instability, the model equations were reformulated in terms of (η, Q), instead of (η, u), where

$$Q = u(h + \eta) \tag{14}$$

as follows:

$$\eta_t + Q_x = 0 \tag{15}$$

$$Q_t + \left(\frac{Q^2}{h+\eta}\right)_x + g(h+\eta)\eta_x + \frac{1}{6}h^3\left(\frac{Q_t}{h+\eta}\right)_{xx} - \left(\frac{1}{2}+\gamma\right)h^2 Q_{txx}$$
$$-\gamma g h^2 (h\eta_x)_{xx} + \frac{f_w|Q|}{2(h+\eta)^2}Q + \epsilon Q = 0 \tag{16}$$

In the course of solving the instability problem, the following numerical schemes were found to be necessary:

1. Use (η, Q) instead of (η, u) as the unknown variables.
2. For the higher-order dispersion term, use $\left(\frac{Q_t}{h}\right)_{xx}$ instead of $\left(\frac{Q_t}{h+\eta}\right)_{xx}$.
3. Express spatial derivative terms containing h in the momentum equation (16) as a Taylor expansion so that no h appears in the denominator, *i.e.*,

$$\frac{h^3}{6}\left(\frac{Q_t}{h}\right)_{xx} = \frac{h^2}{6}Q_{txx} - \frac{1}{3}hh_xQ_{tx} - \frac{1}{6}(hh_{xx} - 2h_x)Q_t. \tag{17}$$

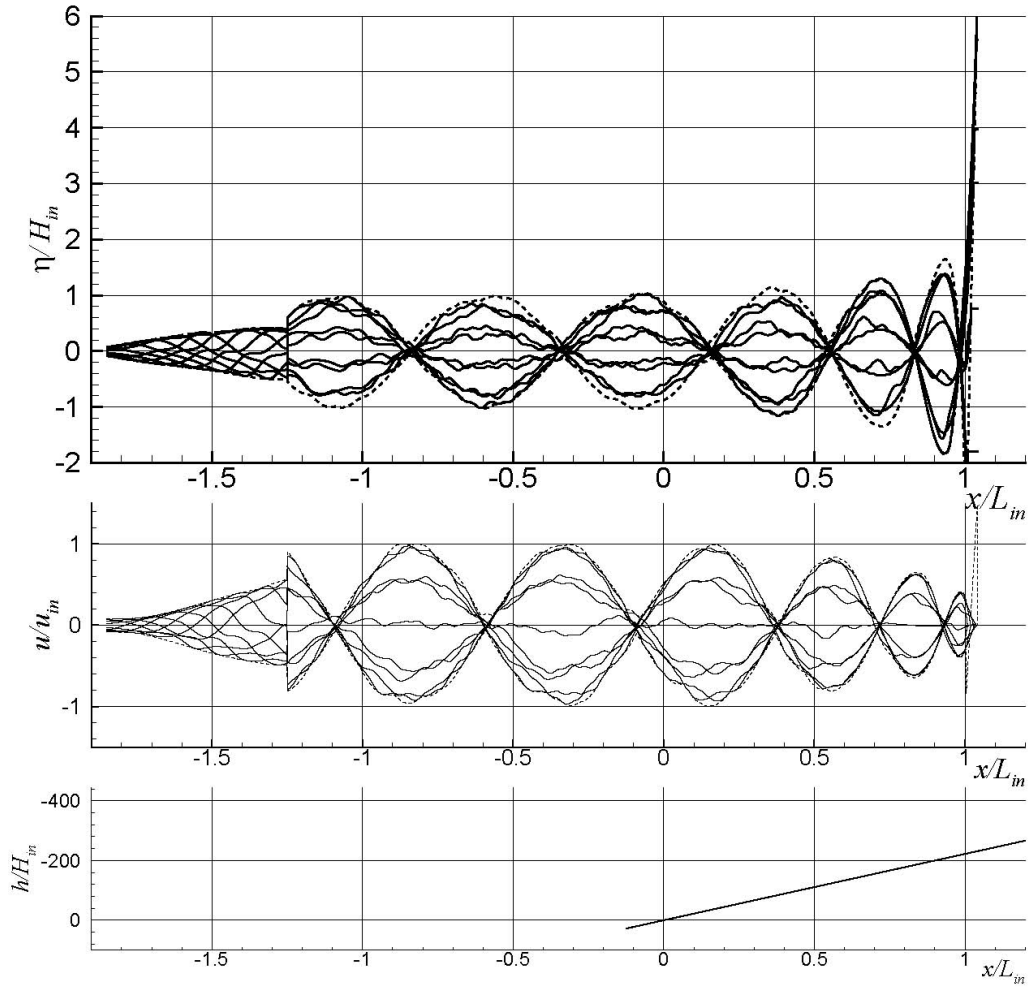

Figure 4. Spatial profiles and envelopes of η and u. Top: $\eta(x)$; Middle: $u(x)$ at intervals of $T_{in}/8$; Bottom: bathymetry of seabed with runup slope. Simulation conditions: $\tan\alpha = 1/30, (H/L)_{in} = 0.00005, (h/L)_{in} = 0.034$. Dashed lines are envelopes of the respective variables.

4. Use a high-accuracy upwind differencing scheme for the nonlinear convective term $(Q^2)_x = 2QQ_x$. The 5-point stencil upwind scheme is adopted in this study *i.e.* with third-order accuracy,

$$Q\frac{\partial Q}{\partial x} = \text{Upwind Scheme} + O(\Delta x^3). \tag{18}$$

5. Solve s^{n+1} by coupling it with η^{n+1} which then requires solution of a cubic equation in s^{n+1}. The coupling results from removing the assumption of parallel slopes of the water elevation at the last wet point, Eq. (7), between successive time steps. The following general relations are instead used:

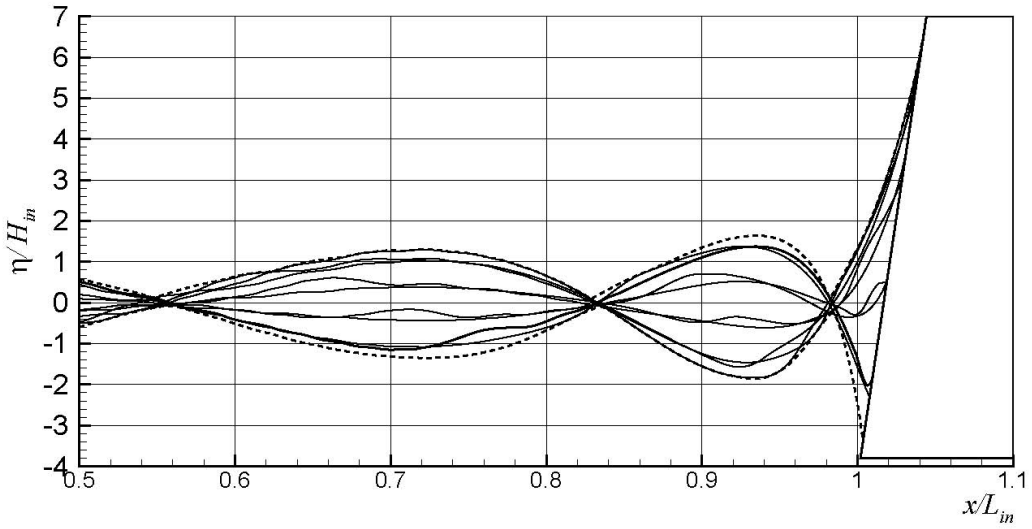

Figure 5. Local conditions of moving shoreline of wave simulation results in Figure 4

$$s^n = -\frac{h+\eta^{n+1}}{\dfrac{\partial h}{\partial x}+\dfrac{\partial \eta^{n+1}}{\partial x}} \tag{19}$$

$$V_1 + V = -\frac{(h+\eta^{n+1})^2}{2\left(\dfrac{\partial h}{\partial x}+\dfrac{\partial \eta^{n+1}}{\partial x}\right)} \tag{20}$$

$$V = Q_0 \Delta t \tag{21}$$

where Q_0 is linearly interpolated based on the last wet point and the shoreline condition

$$Q_{sh} = 0 \tag{22}$$

resulting in

$$Q_0 = \frac{s^n + s^{n+1}}{s^n + s^{n+1} + \Delta x} Q_{NJ-1}^{n+1/2} \tag{23}$$

The updated shoreline position s^{n+1} is still expressed by Eq. (8).
Since V depends on s^{n+1} based on Eq. (21), and s^{n+1} depends on η^{n+1} based on Eq. (19), the solution s^{n+1} is now coupled to η^{n+1}. This coupling leads to a cubic equation in s^{n+1}. Analysis of the real roots of the equation indicates that three cases of wave runup-rundown are possible depending on the coefficients of the cubic equation and the associated real root s^{n+1}. The solution details are discussed in Appendix A.

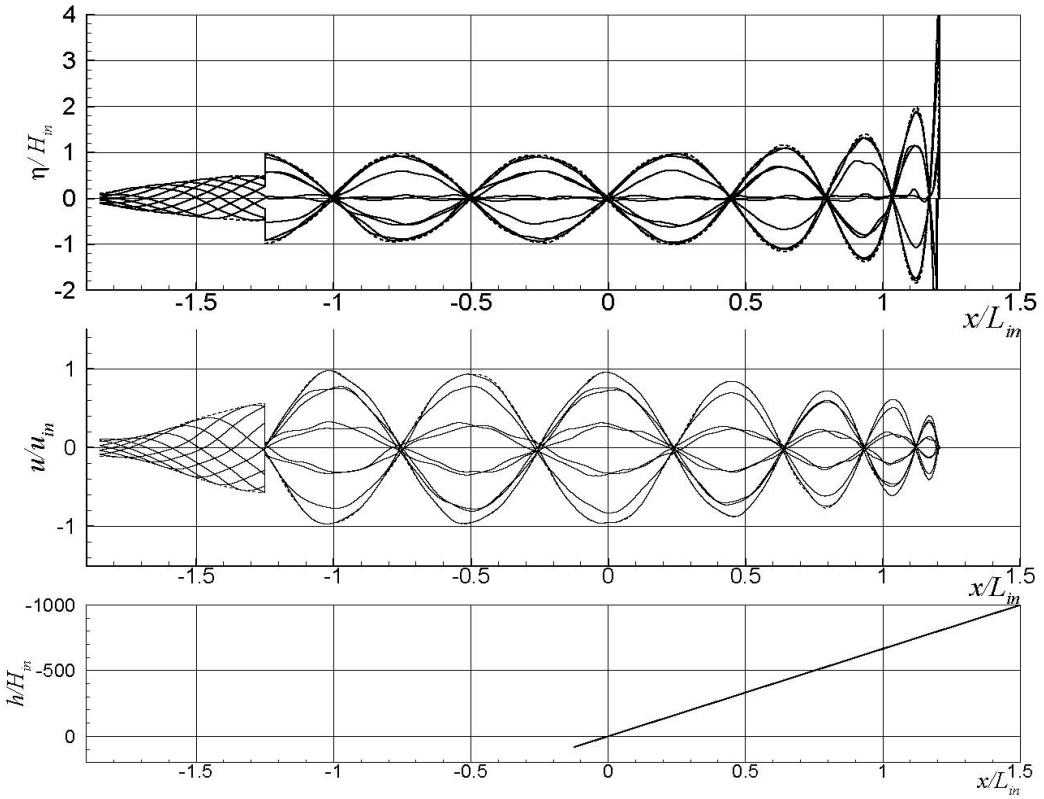

Figure 6. Spatial profiles and envelopes of η and u. Top: $\eta(x)$; Middle: $u(x)$ at intervals of $T_{in}/8$; Bottom: runup slope. Simulation conditions: $\tan\alpha = 1/30, (H/L)_{in} = 0.00005, (h/L)_{in} = 0.040$

6. Use a higher-order scheme for $\dfrac{\partial \eta^{n+1}}{\partial x}$ consistent with the equation for V_1, that is,

$$\begin{aligned} V_1 &= \frac{1}{2}(h + \eta^{n+1})s^n + O(\Delta x^3) \\ \frac{\partial \eta}{\partial x} &= \text{Upwind Scheme} + O(\Delta x^3). \end{aligned} \tag{24}$$

7. Use quadratic interpolation for non-grid values of Q and η.

Figure 6 shows the results of incorporating the above reformulation and numerical treatments. The spatial profiles and envelopes of both η and the new variable Q now show stable forms. The envelopes cover the complete range of the instantaneous water suface shown are thus considered to be stable over time.

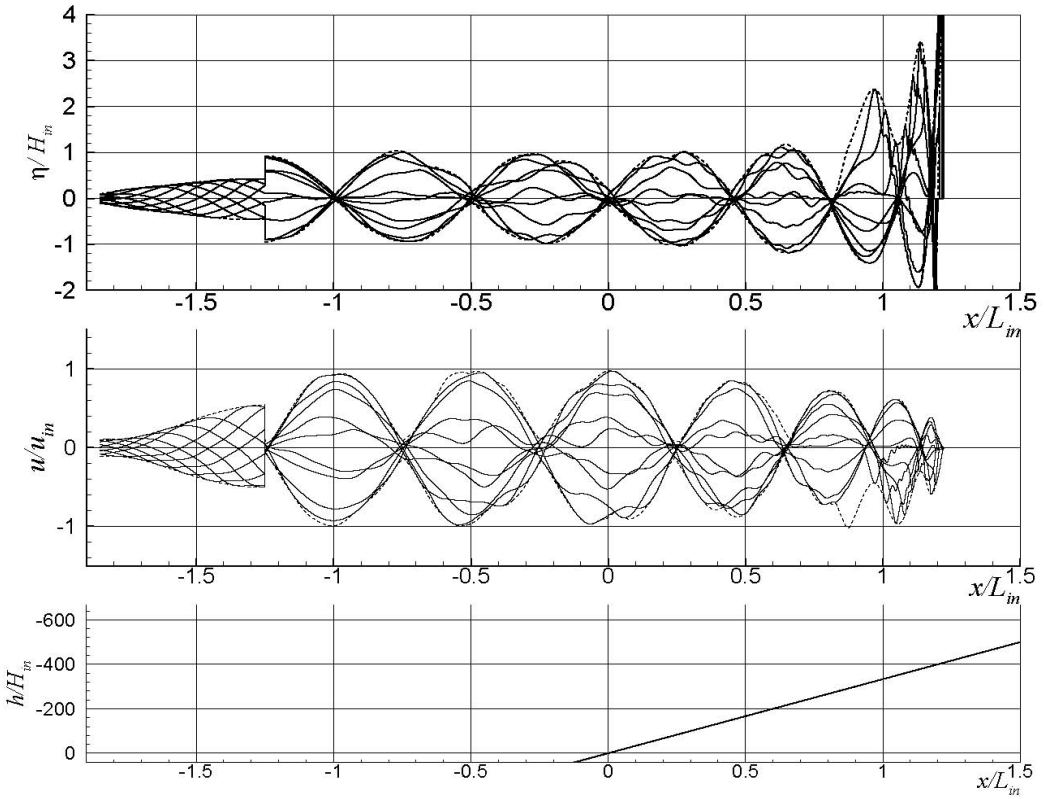

Figure 7. Spatial profiles and envelopes of η and u. Top: $\eta(x)$; Middle: $u(x)$ at intervals of $T_{in}/8$; Bottom: runup slope. Simulation conditions: $\tan\alpha = 1/30, (H/L)_{in} = 0.00010, (h/L)_{in} = 0.040$

6. WAVE SIMULATIONS ON RUNUP SLOPES

In order to test the newly improved shoreline model, a weakly nonlinear incident wave is now considered. The wave nonlinearity is parameterized by the incident wave steepness H/L. The results are shown in Figure 7 for $(H/L)_{in} = 0.00010$, but with similar $(h/L)_{in}$ as in Figure 6. The simulation results show however that instabilities at the shoreline again appear. The induced parasitic waves are now more severe and contaminate the solution for Q. In order to identify the possibly new cause of this instability, the excursion of the shoreline is plotted in Figure 8, after normalization by H_{in}. Apparently, the instability occurs quite abruptly after the excursion amplitude has stabilized after about 9 periods of T_{in}.

Persistent tests of the code's intermediate output revealed that the parasitic waves begin to develop when the total depth D comes close to zero, yet actually is still not zero. The result is a depressed front of the shoreline, which is then amplified by the second-order dispersion terms, namely the third and fourth terms, in the momentum equation (16). Based on this observation, the use of a threshold value D_{th} for D became necessary. In determining the additional active η-grids for the case of wave runup, for example, the last additional η-grid is

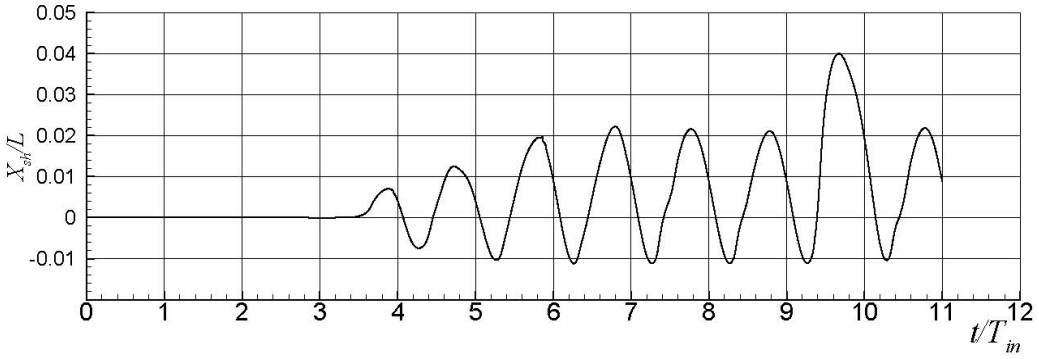

Figure 8. Time series of x_{sh} in Figure 7

where $D > D_{th}$. It becomes necessary to use quadratic interpolation for D as follows:

$$D_{NJ+1} = -\frac{(p_o - p)p}{p_o + 1} D_{NJ-1} + \frac{(p_o - p)(1+p)}{p_o} D_{NJ} \quad \text{for } j = NJ^n + 1, NJ^n + 2, ..., NJ^{n+1} \tag{25}$$

where 2 grid-points $NJ - 1$, NJ are used, and

$$p_o = \frac{s^n}{\Delta x} \qquad p = \frac{(j - NJ)\Delta x}{\Delta x} \tag{26}$$

The aim of such interpolation is to avoid the observed singularity in D which physically corresponds to a depressed front of the shoreline (Figure 9).

Figure 10 shows the results of applying the technique of threshold depth discussed above. It is clear that this numerical scheme effectively removes the instability induced by a depth singularity. Note that the wave steepness of the incident wave is three times that in Figure 7, while the other conditions are identical. Accordingly, the resulting wave runup is smaller when normalized by H_{in}. Also notice that the resulting excursion amplitude of the shoreline is shorter than that in Figure 7, as expected for a nonlinear incident wave with the same dispersivity.

Figure 11 shows the runup-rundown conditions at the slope for the conditions in Figure 10. It is clear that the local spatial profiles are stable and realistically capture the shoreline conditions of the swash motion.

The stability of the improved treatment of singular depths is also verified in Figure 12, which shows a gradual attainment of shoreline excursion amplitude without instability.

The model is verified for runup simulation on a relatively steep beach. It must be recalled that the wave evolution model based on the Boussinesq-type equations is not formally limited by any assumptions on the order of bottom slope and is thus theoretically applicable to steep foreshore faces. In the simulation results shown in Figure 13, the wave conditions are identical to those in Figure 11, except that the runup slope is set to a steep value of 1/20. The plots show stable water surface profiles and spatial envelopes even for this steep slope.

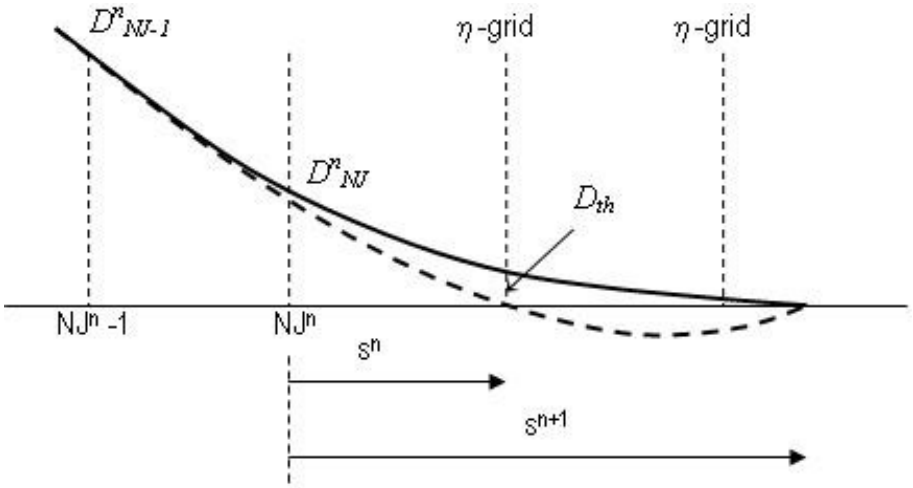

Figure 9. Definition sketch for threshold depth D_{th}. Dashed curve represents uncorrected shoreline front, solid curve for the corrected front.

Figure 14 shows the local wave runup conditions of the profiles in Figure 13. When compared with the simulation results in Figure 5, the (normalized) runup on a steep slope is smaller than that for a milder slope. This is in agreement with theory (Mei [9]) and empirical data (Shore Protection Manual [10]).

The evolution of the shoreline excursion shown in Figure 15 does not manifest time instabilities and the excursion amplitude steadies after a few periods from cold start. Figure 13 indicates that the runup elevation is smaller than that for a mild slope (Figure 6), which is qualitatively correct. Also, the spatial envelopes show fewer number of quasi-nodes within the slope compared to that in Figure 11. This is consistent with the theoretical results of nonlinear wave theory (Mei [9]).

In addition to simulating the wave propagation and swash motions on runup slopes, the present moving shoreline model also provides a means of determining the magnitude of the swash-induced reflected wave from the slope. By computing the height of the spatial envelopes of η just seaward of the wave source $x = x_s$, the height of the wave reflected at the slope due to the moving shoreline can be determined. Based on Figures 6 and 10, for example, we see that the wave reflected by a steeper incident wave (Figure 10) is higher than that by a milder wave (Figure 6) on the same runup slope. This agrees with theoretical results (Carrier and Greenspan [11]) and experimental data (Shore Protection Manual [10]).

7. CONCLUSIONS

The cross-shore wave evolution model of Cruz et al. (1997) based on variables (η, u) is capable of predicting the nonbreaking runup-rundown motion of the shoreline. This is primarily because the model equations contain the leading order of wave nonlinearity and is thus valid for the shallow waters in the zone of the moving shoreline.

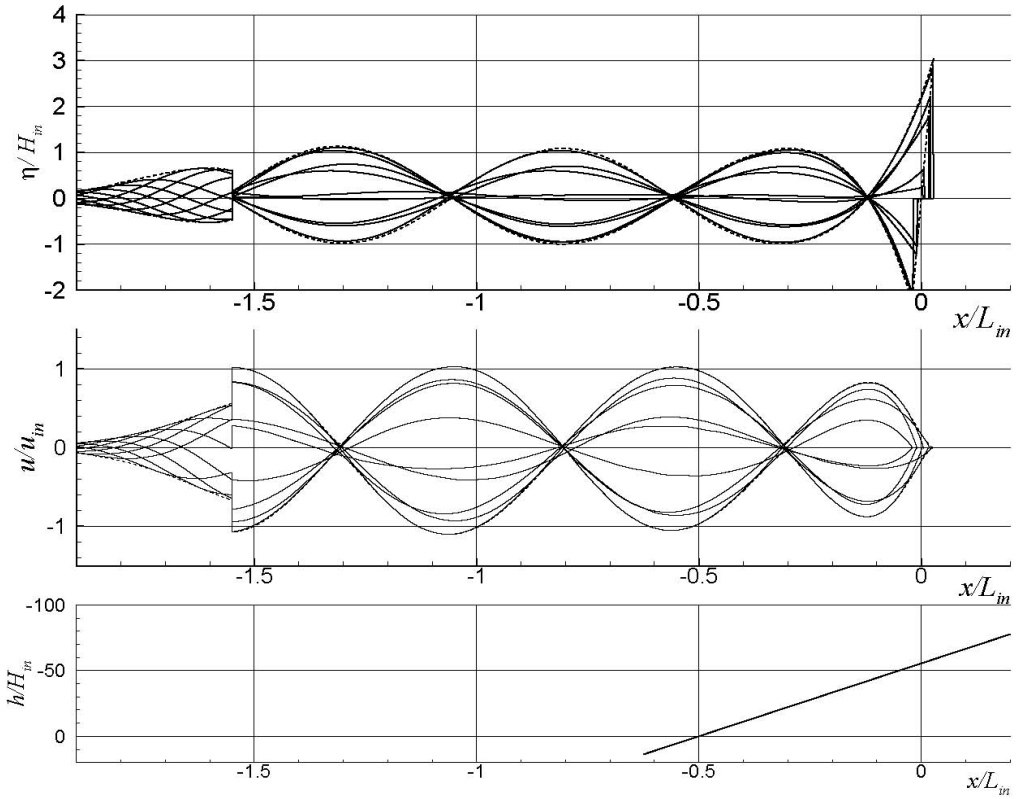

Figure 10. Spatial profiles and envelopes of η and u. Top: $\eta(x)$; Middle: $u(x)$ at intervals of $T_{in}/8$; Bottom: runup slope. Simulation conditions: $\tan\alpha = 1/30, (H/L)_{in} = 0.00030, (h/L)_{in} = 0.040$

The moving shoreline condition is formulated using the concept of net volume change of the water contained in the last wet point of the shoreline front. Numerical discretization is implemented on fixed spatial grids for ease in coding. However, this fixed grid exposes the shoreward grid points to alternate inundation and drying conditions that cause numerical instabilities. Recasting the model equations from (η, u) to (η, Q) together with higher-order differencing schemes solves this instability problem. It is also necessary to maintain the coupling of the unknown shoreline position s^{n+1} and updated water displacement η^{n+1} at the last wet point.

Application of the reformulated model to steeper incident waves causes parasitic waves to emerge from the shoreward grid points, which has been traced to singularities caused by too small total depth at the last wet point. This new instability is suppressed by introducing a threshold value at the last wet point. The technique appears to be effective not only for nonlinear incident waves but also for steeper runup slopes.

The envelopes and spatial profiles of the simulated water surface agree with the analytical results of past studies for nonbreaking waves. The local conditions of wave runup and shoreline-induced reflected wave also agree qualitatively with theory and empirical data.

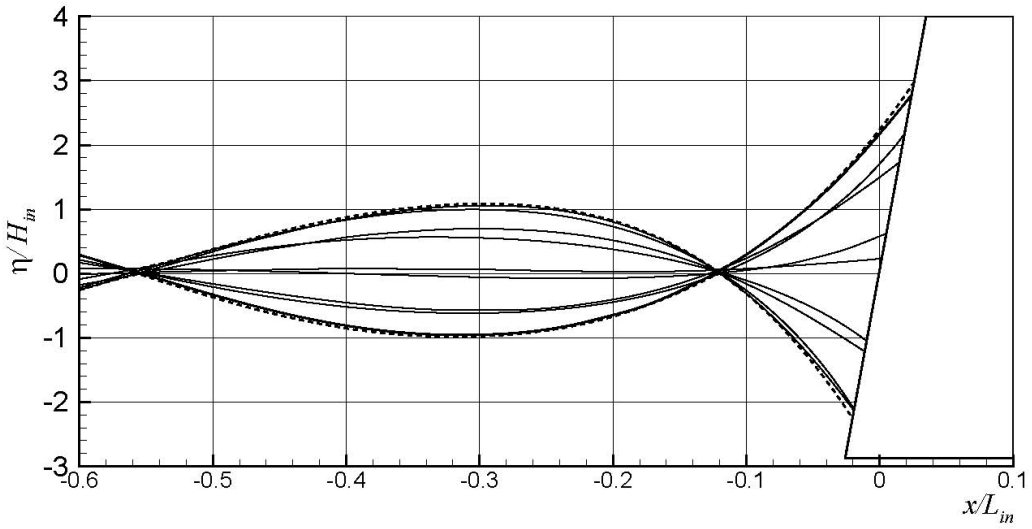

Figure 11. Local conditions of moving shoreline of wave simulation results in Figure 10

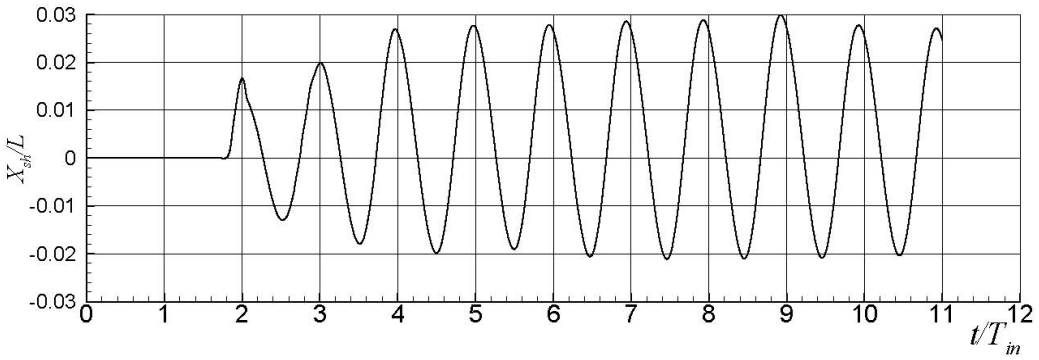

Figure 12. Time series of x_{sh} in Figure 11

ACKNOWLEDGEMENTS

This study was supported by the Office of the Vice President for Academic Affairs under a University of the Philippines System Research Grant, Creative and Research Scholarship Fund 2003-04. The research was undertaken at the College of Engineering, U.P. Diliman.

REFERENCES

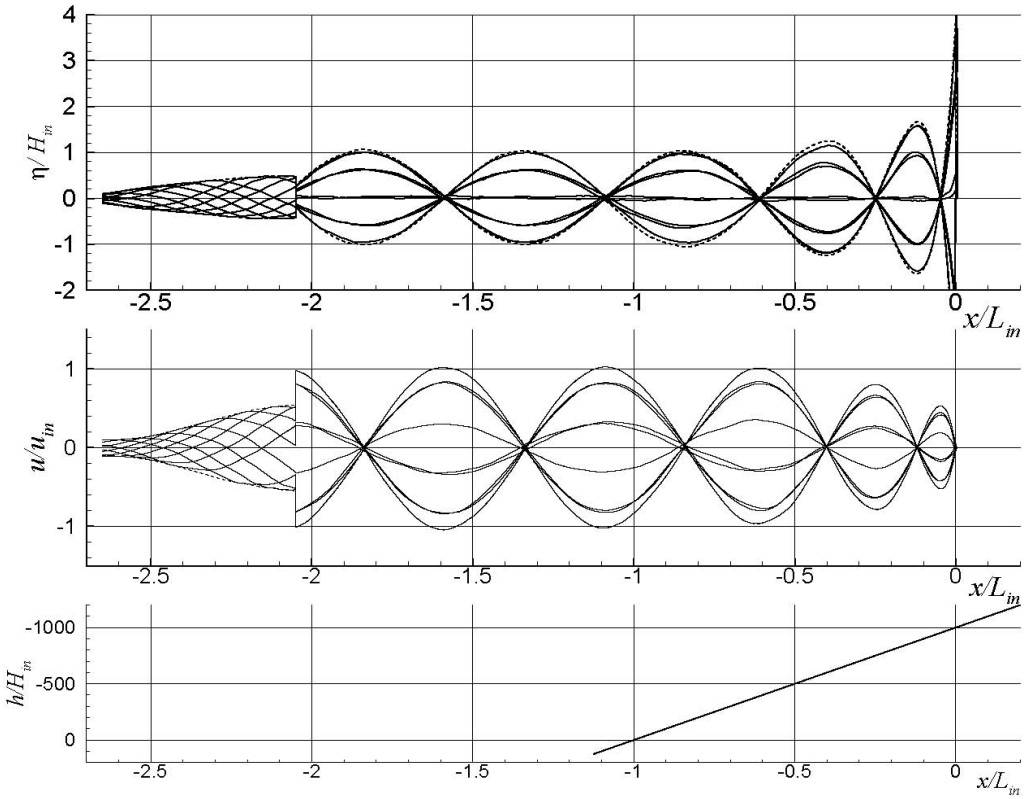

Figure 13. Spatial profiles and envelopes of η and u. Top: $\eta(x)$; Middle: $u(x)$ at intervals of $T_{in}/8$; Bottom: runup slope. Simulation conditions: $\tan\alpha = 1/20, (H/L)_{in} = 0.00005, (h/L)_{in} = 0.040$

1. M. Brocchini, and D.H. Peregrine: *Integral flow properties of the swash zone and averaging.* Jour. Fluid Mech., Vol. 317, 241-273 (1996)
2. S. Hibberd and D.H. Peregrine: *Surf and runup on a beach: a uniform bore.* Jour. of Fluid Mech., Vol. 95, 323-345 (1979)
3. N. Kobayashi and B.D. Johnson, B.D.: *Numerical model VBREAK for vertically two-dimensional breaking waves on impermeable slopes.* Research Report CACR-95-06, Univ.of Delaware, 66 pages (1995)
4. R.O. Reid and B.R. Bodine: *Numerical model for storm surges in Galveston Bay.* Jour. of the Waterways and Harbors Division, Proc. ASCE, Vol. 94, WW1, 33-57 (1968)
5. E.C. Cruz, M. Isobe and A. Watanabe: *Boussinesq equations for wave transformation on porous beds.* Coastal Engineering, Vol. 30, Nos 1-2, 125-156 (1997)
6. T. Ishii, M. Isobe and A. Watanabe: *Improved boundary conditions to a time-dependent mild-slope equation for random waves.* Proc., 24th International Conference Coastal Engineering, ASCE, 272-284 (1994)
7. A.B. Kennedy, Q. Chen, J.T. Kirby and R.A. Dalrymple: *Boussinesq modeling of wave transformation, breaking, and runup. I: 1D.* Jour. Waterway, Port, Coastal, and Ocean Engineering, Vol.26, No.1, Jan/Feb (2000)
8. E.C. Cruz: *Final Report: Theoretical Analysis of Wave Absorptiom Method and Numerical Simulation of Wave Fields on Open Coasts.* Research Report submitted to Univ. of the Phils. - Office of the Vice-Chancellor for Research and Development (2003)
9. C.C. Mei: *The Applied Dynamics of Ocean Surface Waves.* World Scientific Publishing (1989)
10. Coastal Engineering Research Center: *Shore Protection Manual, Fourth Edition.* U.S. Government Printing Office (1984)

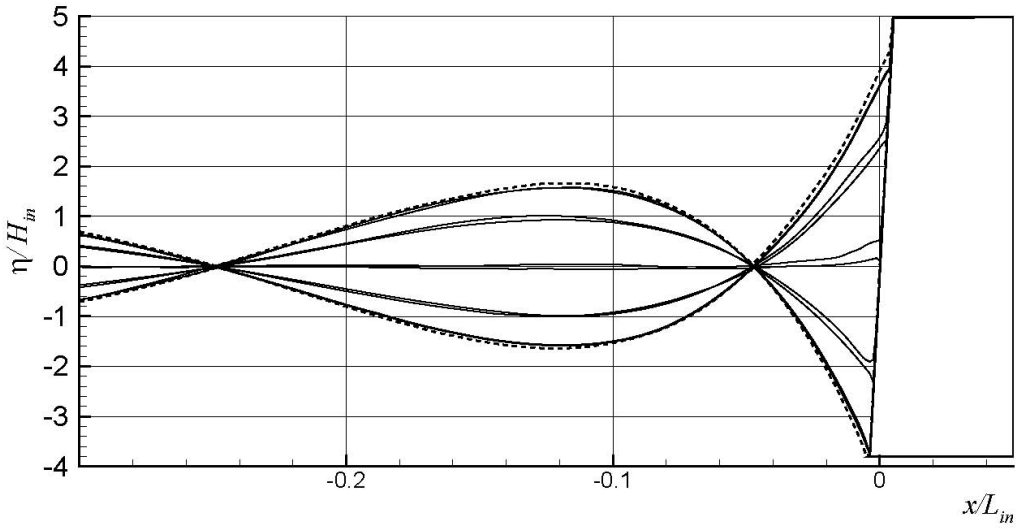

Figure 14. Local conditions of moving shoreline of wave simulation results in Figure 13

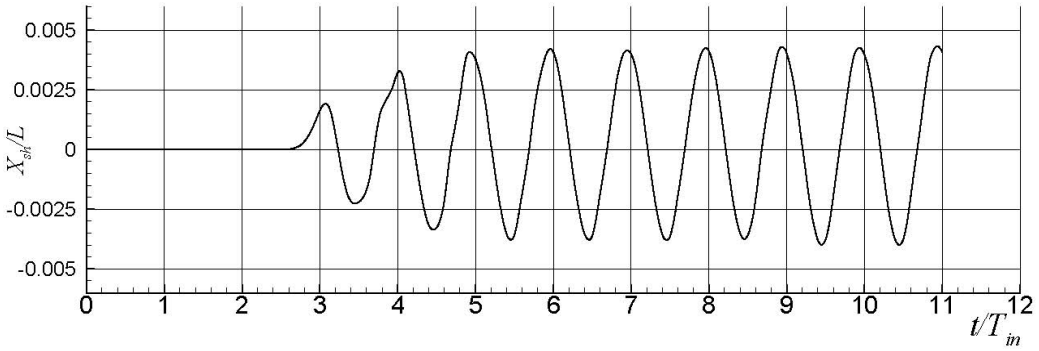

Figure 15. Time series of x_{sh} in Figure 14

11. G.F. Carrier and H.P. Greenspan: *Water waves of finite amplitude on a sloping beach.* Jour. Fluid Mechanics, No.4, Part 1, 97-109 (1958)
12. P.A. Madsen and O.R. Sorensen: *A new form of Boussinesq equations with improved linear dispersion characteristics.* Coastal Engg., Vol.15. 371-388 (1991)
13. M. Isobe, K. Shiba, E.C. Cruz and A. Watanabe: *On the transformation of nonlinear waves around submerged permeable structures.* Proc., 38th Coastal Eng. Conf., JSCE, Vol 2, 551-555 (in Japanese) (1992).
14. M. Abramowitz and I.E. Stegun (eds.): *Handbook of Mathematical Functions.* National Bureau of Standards, U.S. Government Printing Office (1964).

APPENDIX

A. COUPLED SOLUTION OF SHORELINE POSITION

Let

$$z = s^{n+1} \tag{27}$$

With s^{n+1} contained in Q_0 of Eq. (23), Eq. (20) is substituted into Eq. (8), η^{n+1} is eliminated in the resulting equation and Eq. (19), leading to the cubic equation

$$z^3 + Az^2 + Bz + c = 0 \tag{28}$$

where

$$A = s^n + \Delta x \tag{29}$$

$$B = \frac{2(V_1 + V)}{D_x^n} \tag{30}$$

$$C = \frac{2}{D_x^n}[s^n(V_1 + V) + V_1\Delta x] \tag{31}$$

in which

$$D_x = \frac{\partial}{\partial x}(h + \eta)$$

To obtain the possible roots of Eq. (29), let

$$q = \frac{1}{3}B - \frac{1}{9}A^2 \tag{32}$$

$$r = \frac{1}{6}(AB - 3C) - \frac{1}{27}A^3. \tag{33}$$

Then there are 3 possible cases for the roots of Eq. (28) (Abramowitz and Stegun [14]):

1. If $q^3 + r^2 > 0$: one real root and a pair of complex conjugate roots .
2. If $q^3 + r^2 = 0$: all roots are real and at least two are equal.
3. If $q^3 + r^2 < 0$: all roots are real (irreducible case).

By further analyzing the expression $(q^3 + r^2)$, it is concluded that there are 3 possible solutions when the roots are real-valued, as follows:

1. Uprush/downrush without LWP movement: occurs when $q^3 + r^2 > 0$ and $0 < s^{n+1} \leq \Delta x$
2. Uprush with LWP shoreward movement: occurs when $q^3 + r^2 > 0$ and $s^{n+1} > \Delta x$
3. Downrush with LWP seaward movement: occurs when $q^3 + r^2 < 0$ and $s^{n+1} < \Delta x$

B. NOMENCLATURE

Symbol description

η	water surface displacement(m)
u	depth-averaged fluid particle horizontal velocity (m/s)
h	local water depth measured from still-water level (m)
D	local total depth (m)
x	cross-shore direction (m)
t	time (s)
g	gravitational acceleration (=9.806 m/s^2)
γ	dispersivity factor (dimensionless)
f_w	wave friction factor (dimensionless)
ϵ	boundary damping coefficient (s^{-1})
Q	wave-induced oscillatory flow rate (m^3/s)
V	volume of water contained in the last wet grid point (m^3)
s	shoreline position (m)
Δx	grid spacing (m)
Δt	time step (s)
x_s	location of source generator (m)
x_o	location of last wet point (m)
n	time level
j	spatial grid index
NJ	grid index of last wet point
H	wave height (m)
L	wavelength (m)
T	wave period (s)
C	wave celerity (m/s)
$O(\ )$	"Order of ( )"

Subscript and abbreviation

in	incident wave
out	outgoing wave
sh	shoreline
th	threshold value
LWP	last wet point

